ЖЭТФ, 2013, том 144, вып. 1 (7), стр. 161–165

ELECTRONIC STRUCTURE OF ZrO_2 USING COMPTON SPECTROSCOPY

F. M. Mahammad [a], ***S. F. Mahammed*** [a], ***R. Kumar*** [b], ***Y. K. Vijay*** [b], ***B. K. Sharma*** [b], ***G. Sharma*** [c*]

[a] *Department of Physics, University of Tikrit 42, Iraq*

[b] *Department of Physics, University of Rajasthan, Jaipur 303001, India*

[c] *Department of Pure and Applied Physics, University of Kota, Kota 324010, India*

Received December 14, 2012

The electronic structure of ZrO_2 is reported using the Compton scattering technique. The first-ever Compton profile measurement on polycrystalline ZrO_2 was made using 59.54 keV gamma-rays emanating from the ^{241}Am radioisotope. To explain the experimental data, we compute theoretical Compton profile values using the method of linear combination of atomic orbitals in the framework of density functional theory. The correlation scheme proposed by Perdew–Burke–Ernzerhof and the exchange scheme of Becke are considered. The ionic-model-based calculations for a number of configurations, i. e., $Zr^{+x}(O^{-x/2})_2$ $(0 \le x \le 2)$, are also performed to estimate the charge transfer on compound formation, and the study supports transfer of 1.5 electrons from Zr to O atoms.

DOI: 10.7868/S004445101307016X

1. INTRODUCTION

Zirconium dioxide ZrO_2 is one of the most studied transition metal oxide systems due to many practical applications in gas sensors, fuel cells, catalysis, paint additives, and high durability coating and ceramics [1–6]. An increasing number of these applications demands a more fundamental understanding of the electronic structure of this material. At ambient pressure, ZrO_2 has three polymorphs, the monoclinic ($P2_1/c$, C_{2h}^5) at temperatures below 1170 °C, the tetragonal ($P4_2/nmc$, D_{4h}^{15}) at temperatures from 1170 to 2370 °C, and the cubic fluorite ($Fm3m$, O_h^5) at temperatures from 2370 to 2680 °C. The monoclinic structure, i. e., m-ZrO_2 (Fig. 1), has a wide range of temperature and is stable under ambient conditions [7].

A number of researchers have investigated the electronic, structural, and optical properties of ZrO_2. The electronic structure and bonding of m-ZrO_2 were reported in [7] using the plane-wave ultrasoft pseudopotential technique based on the first-principle density functional theory (DFT). Monoclinic ZrO_2 was found to have an indirect band gap with 3.65 eV and a direct

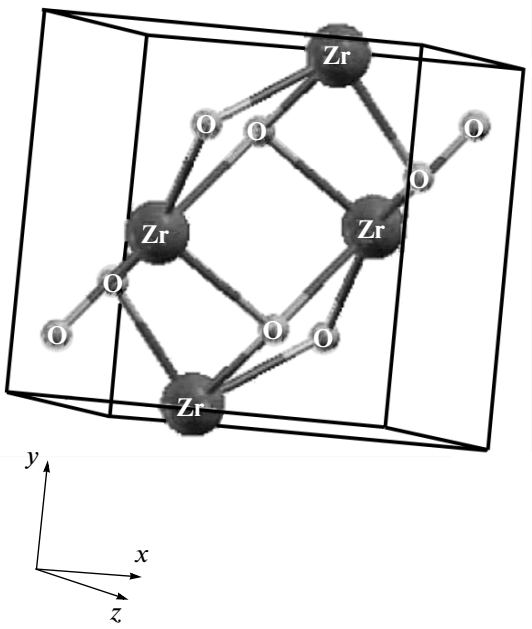

Fig. 1. Monoclinic lattice structure of ZrO_2

*E-mail: gsphysics@gmail.com

gap with 4.05 eV. The electronic properties of ZrO_2 for the cubic, tetragonal, and monoclinic crystalline phases were investigated in [8] using all-electron full-potential linear augmented plane-wave method. The authors of [8] observed that the carrier effective masses are highly anisotropic with the relativistic corrections. The plane-wave based DFT was used in [9] to explore the structural and electronic properties of ZrO_2 in the range of pressures from 0 to 50 GPa. In [10], an *ab initio* constant-pressure technique was used to investigate the high-pressure behavior of m-ZrO_2 up to 140 GPa. The structural phase transition in ZrO_2 was reported in [11] based on pseudopotential plane-wave methods within the Perdew–Burke–Ernzerhof (PBE) form of the generalized gradient approximation (GGA). Phase transitions from monoclinic to ortho-I and from ortho-I to ortho-II were found at 7.94 GPa and 11.58 GPa. The phase relations and mechanical hardness of m-ZrO_2 under pressure were reported in [12] using high-resolution synchrotron X-ray powder diffraction and the DFT. The static dielectric properties and Raman spectra under pressure were investigated in [3] for several polymorphs of ZrO_2. Although studies of electronic properties are performed on m-ZrO_2, the ground-state properties like the electron momentum density and Compton profile are rarely addressed within experimental and first-principle methods. Therefore, we find the electronic structure of m-ZrO_2 with the Compton profile perspectives worthy of study.

It is well known that the Compton scattering technique is a powerful tool in exploring the ground-state properties of solids [14, 15]. In this technique, the Compton profile, $J(p_z)$, which is the projection of the electron momentum density along the scattering vector is defined as

$$J(p_z) = \iint \rho(p_x, p_y, p_z)\, dp_x dp_y, \qquad (1)$$

where $\rho(p_x, p_y, p_z)$ is the electron momentum density, which can be derived by transforming the real space electron wave-function into momentum space.

To explore the electronic structure of m-ZrO_2, we report the measurement of the Compton profile. The decision to measure the isotopic Compton profile was due to nonavailability of large-size (diameter 18 mm, thickness 3 mm) single crystals of ZrO_2. To compare our experimental data, we have computed the Compton profile using the method of linear combination of atomic orbitals (LCAO). Further, the ionic model has also been used to estimate the charge transfer in m-ZrO_2. In this paper, unless stated otherwise, all quantities are in atomic units (a.u.) with $e = \hbar = m = 1$ and $c = 137.036$, giving the unit momentum $1.9929 \cdot 10^{-24}$ kg·m/s, unit energy 27.212 eV, and unit length $5.2918 \cdot 10^{-11}$ m.

2. EXPERIMENTAL DETAILS AND DATA ANALYSIS

The Compton profile of polycrystalline ZrO_2 has been measured using 5Ci ^{241}Am Compton spectrometer [16]. The high-purity (more than 99.99 %) ZrO_2 sample of thickness 3.2 mm and effective density 1.37 g/cm^3 was used in the measurement. The powder sample was placed in a circular cell with mylar windows on both the front and the back sides. A brass sample holder with a circular opening of 18 mm in diameter, masked with lead, was used to mount the sample. To reduce the contribution of air scattering, the sample was placed in a chamber evacuated to about 10^{-2} Torr with a rotary oil pump. The scattered photons, at a prefixed scattering angle of $166 \pm 3.0°$, were detected and analyzed using an HPGe detector (Canberra, GL0110P model) and associated electronics like a spectroscopy amplifier (Canberra, 2020 model), an analogue-to-digital converter (Canberra, 8701 model), and a multichannel analyzer (Canberra, S-100). The channel width of the multichannel analyzer (4096 channels) was 20 eV, corresponding to 0.03 a.u. of the momentum scale. The calibration of the spectrometer was checked regularly using a weak ^{241}Am source.

After removing the sample from the sample holder, the background was measured and subtracted from the raw data point by point after scaling it to the actual counting time. The measured profile was then corrected for the effects of the detector response function, energy dependent absorption, and scattering cross section using the computer code of the Warwick group [17, 18]. The overall momentum resolution of the spectrometer was 0.6 a.u. (Gaussian, FWHM). Using a Monte Carlo simulation [18], the experimental data were corrected for the multiple scattering effects. Finally, the Compton profile was normalized to 24.071 electrons, which is the free atom profile area in the momentum range 0 to +7 a.u. [19] excluding the contribution of 1s electrons in Zr.

3. THEORETICAL DETAILS

3.1. DFT-LCAO method

To compute the theoretical Compton profile of m-ZrO_2, the LCAO method embodied in the

CRYSTAL06 code [20, 21] was used, which provided a platform to calculate the electronic structure of the periodic system considering Gaussian basis sets. In the LCAO method, each crystalline orbital is built from a linear combination of Bloch functions. The Bloch functions are defined in terms of local functions constructed from a certain number of atom-centered Gaussian functions. For Zr and O, the local functions were constructed from Gaussian-type basis sets [22]. In the present DFT calculation, the crystal Hamiltonian was generated using the PBE correlation functional [23] and the exchange scheme of Becke [24]. The computation was performed with m-ZrO_2 (see Fig. 1), which is stable at ambient conditions, with lattice constants $a = 5.15$ Å, $b = 5.21$ Å, and $c = 5.32$ Å and space group $P2_1/c$, C_{2h}^5. The calculation was performed by considering 170 **k** points as the irreducible wedge of the Brillouin zone.

3.2. Ionic model

The theoretical Compton profile of m-ZrO_2 for different ionic configurations was calculated from the free-atom Compton profiles of Zr and O atoms taken from [19]. The valence profiles for various $Zr^{+x}(O^{-x/2})_2$ $(0 \le x \le 2)$ configurations were computed by transferring x electrons from the $5s$ shell of Zr to the $2p$ shell of the O atom. The valence profiles for $Zr^{+x}(O^{-x/2})_2$ configurations were then added to the core contribution to obtain the total profile. All the profiles were then appropriately normalized to compare with the measured profile of m-ZrO_2.

4. RESULTS AND DISCUSSION

The numerical values of the unconvoluted spherically averaged theoretical Compton profile (DFT-LCAO) of m-ZrO_2 are presented in the Table. The ionic profiles, derived from the free-atom model considering various ionic arrangements, e. g., $Zr^{+x}(O^{-x/2})_2$ $(0 \le x \le 2)$, are also included. The experimental Compton profile of the compound is given in the last column of the Table including experimental errors at selected points.

We have computed the directional Compton profiles of m-ZrO_2 along [100], [110], and [001] directions to examine the [100]–[110], [100]–[001], and [110]–[001] anisotropies in the electron momentum density. We present all these anisotropies derived from a convoluted DFT-PBE scheme in Fig. 2. The figure depicts that the [100]–[110] and [100]–[001] anisotropies are positive in nature, but the [110]–[001] anisotropy is negative around $p_z = 0$ a.u. This indicates larger occupied states along the [100] direction with a low momentum. A close inspection of this figure reveals that the maximum anisotropy is seen between [110] and [001] directions at 1.6 a.u. All anisotropies are visible up to 4.0 a.u. Measurements on single-crystal samples of m-ZrO_2 along principal directions would be valuable to examine these computed anisotropies.

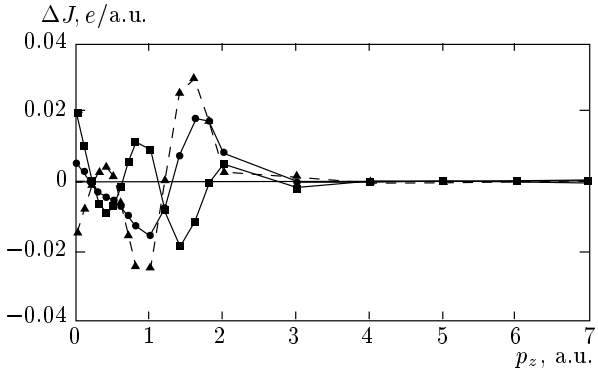

Fig. 2. Directional anisotropies $\Delta J(p_z)$ for ZrO_2 for the pairs of directions [100]–[110] (■), [100]–[001] (•), and [110]–[001] (▲)

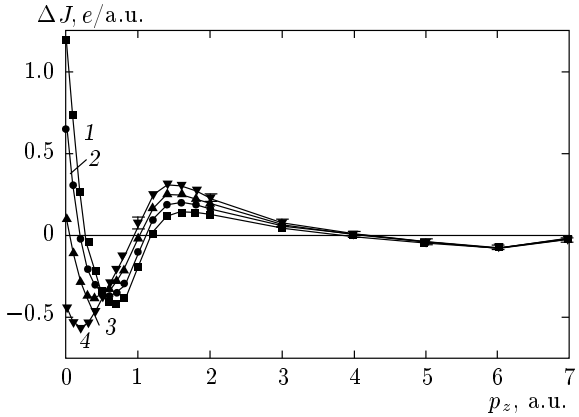

Fig. 3. The difference ΔJ between convoluted ionic and experimental Compton profiles of ZrO_2: curve *1* — $Zr^{+0.5}(O^{-0.25})_2$; *2* — $Zr^{+1.0}(O^{-0.5})_2$; *3* — $Zr^{+1.5}(O^{-0.75})_2$; *4* — $Zr^{+2.0}(O^{-1.0})_2$. Experimental errors $\pm\sigma$ are also shown at the points. All ionic profiles are convoluted with the Gaussian of 0.6 a.u. FWHM

In Fig. 3, the experimental Compton profile of m-ZrO_2 is compared with various ionic arrangements. A similar approach has also been used to estimate the charge transfer in many compounds [25–28]. For a quantitative comparison of the ionic computation and

Table. Unconvoluted theoretical (DFT-LCAO and ionic) and experimental Compton profiles of ZrO_2. All profiles are normalized to 24.071 electrons in the range 0–7 a.u. Statistical errors ($\pm\sigma$) are also given at some points

p_z, a.u.	$J(p_z)$, e/a.u.					
	DFT-LCAO	Ionic model				Experiment
		$Zr^{+0.5}(O^{-0.25})_2$	$Zr^{+1.0}(O^{-0.5})_2$	$Zr^{+1.5}(O^{-0.75})_2$	$Zr^{+2.0}(O^{-1.0})_2$	
0	12.004	14.556	13.833	13.110	12.386	12.668 ± 0.044
0.1	11.969	14.185	13.573	12.960	12.346	12.620
0.2	11.850	13.280	12.921	12.563	12.204	12.450
0.3	11.656	12.313	12.199	12.085	11.970	12.150
0.4	11.375	11.498	11.538	11.578	11.617	11.736
0.5	11.029	10.837	10.946	11.056	11.165	11.229
0.6	10.613	10.225	10.351	10.479	10.606	10.651
0.7	10.126	9.611	9.734	9.857	9.981	10.010
0.8	9.503	8.935	9.032	9.130	9.227	9.321
1.0	8.274	7.629	7.721	7.812	7.904	7.870 ± 0.033
1.2	6.819	6.374	6.449	6.525	6.601	6.496
1.4	5.499	5.338	5.401	5.463	5.525	5.376
1.6	4.470	4.514	4.565	4.616	4.666	4.517
1.8	3.780	3.888	3.928	3.968	4.008	3.868
2.0	3.331	3.419	3.451	3.482	3.513	3.385 ± 0.020
3.0	2.272	2.270	2.279	2.286	2.294	2.229 ± 0.016
4.0	1.681	1.679	1.682	1.684	1.686	1.682 ± 0.013
5.0	1.221	1.221	1.222	1.223	1.223	1.263 ± 0.011
6.0	0.866	0.867	0.867	0.867	0.868	0.947 ± 0.009
7.0	0.652	0.653	0.653	0.653	0.653	0.693 ± 0.007

experiment, the difference profiles $\Delta J = J^{theor}(p_z) - J^{exp}(p_z)$ have been deduced after convoluting all ionic profiles with a Gaussian function with a 0.6 a.u. FWHM. All ionic values are normalized to 24.071 electrons in the momentum range 0 to +7 a.u. The figure depicts that the effect of charge transfer from Zr to O atoms is largely visible within 0–3.0 a.u. and the ionic configuration with $x = 0.5$ shows the largest deviation from the experiment around $J(0)$. The best agreement is found for $x = 1.5$. Beyond 3.0 a.u., all configurations show identical behavior and all curves overlap with each other. On the basis of χ^2 checks and from Fig. 3, it is found that the $Zr^{+1.5}(O^{-0.75})_2$ configuration gives the best agreement among the ionic arrangements, suggesting the transfer of 1.5 electrons from the valence $5s$ state of the Zr atom to the $2p$ states of the O atoms. In [29], the GGA-PBE scheme was used to describe the interactions among valence electrons of Zr and O, and the transfer of 1.5 electrons from Zr to O atoms was also observed there.

Next, in Fig. 4, we compare the total experimental and DFT-PBE scheme based Compton profiles. The difference $\Delta J = J^{theor}(p_z) - J^{exp}(p_z)$ between two data is also presented in the inset of the figure. Similar structures are also seen in the difference curves of Zr and ZrB_2 solids [30]. The maximum difference shown by the DFT-PBE with the experimental $J(0)$ value is about 4.73 %. The figure indicates that the DFT-PBE scheme underestimates the electron momentum density in the momentum range $0 < p_z < 0.5$ a.u., while the trend is reversed in the momentum range $0.5 < p_z < 2.0$ a.u. The difference between two data is negligible in the high-momentum region because the contribution in this region is mostly due to core electrons, which remain unaffected in the solid formation.

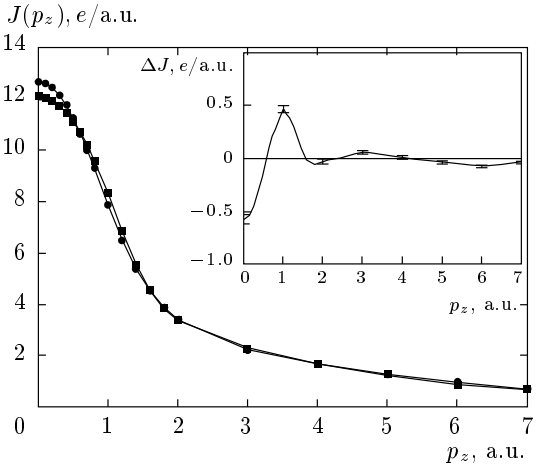

Fig. 4. The absolute DFT-LCAO (■) and experimental (•) Compton profiles of ZrO_2. The inset shows the difference between two data. Both profiles are convoluted with the Gaussian of 0.6 a.u. FWHM

5. CONCLUSIONS

The electronic structure of polycrystalline m-ZrO_2 is studied using the Compton scattering technique. The experimental values of the Compton profile are compared with the DFT-LCAO-based values. The anisotropies in momentum densities depict larger occupied states along the [100] direction with low momentum. In addition, the ionic-model-based calculations have also been used to estimate the charge transfer in the compound, and the model suggests a transfer of 1.5 electrons from the $5s$ state of the Zr atom to the $2p$ state of the O atoms.

The authors are thankful to the Head, Department of Pure and Applied Physics, University of Kota for providing the computational facilities. This work is financially supported by the CSIR, New Delhi through the grant No. 03(1205/12EMR-II).

REFERENCES

1. J. Hong, R. Patrick, and S. Matthias, Phys. Rev. B **81**, 085119 (2010).
2. Y. Deok, J. S. Hyung, K. H. Jeong, and H. S. Cheol, Appl. Phys. Lett. **97**, 141905 (2010).
3. E. Dela, L. A. Diaz-Torres, P. Salas et al., J. Phys. D **34**, 83 (2001).
4. L. D'Souza, A. Suchopar, K. Zhu et al., Micro. Meso. Mater. **88**, 22 (2006).
5. S. Zhao, F. Ma, K. W. Xu, and H. F. Liang, J. Alloys Comp. **453**, 453 (2008).
6. G. Dutta and U. V. Waghmare, Sol. St. Comm. **146**, 495 (2008).
7. Qi-Jun Liu, Zheng-Tang Liu, and Li-Ping Feng, Physica B **406**, 345 (2011).
8. J. C. Garcia, L. M. R. Scolfaro, A. T. Lino et al., Appl. Phys. **100**, 104103 (2006).
9. V. Milman, A. Perlov, K. Refson et al., J. Phys: Condens. Matter **21**, 485404 (2009).
10. H. Ozturk and M. Durandurdu, Phys. Rev. B **79**, 134111 (2009).
11. H. Ren, B. Zhu, J. Zhu et al., Sol. St. Sci. **13**, 938 (2011).
12. Y. Al-Khatatbeh, K. K. M. Lee, and B. Kiefer, Phys. Rev. B **81**, 214102 (2010).
13. G. Fadda, G. Zanzotto, and L. Colombo, Phys. Rev. B **82**, 064106 (2010).
14. M. J. Cooper, P. E. Mijnarends, N. Shiotani, N. Sakai, and A. Bansil, *X-Ray Compton Scattering*, Oxford Publ. Press, Oxford (2004).
15. M. J. Cooper, Rep. Prog. Phys. **48**, 415 (1985).
16. B. K. Sharma, A. Gupta, H. Singh et al., Phys. Rev. B **37**, 6821 (1988).
17. D. N. Timms, Ph. D. Thesis (unpublished), University of Warwick, UK (1989).
18. J. Felsteiner, P. Pattison, and M. J. Cooper, Phil. Mag. **30**, 537 (1974).
19. F. Biggs, L. B. Mandelsohn, and J. B. Mann, At. Data Nucl. Data Tables **16**, 201 (1975).
20. R. Dovesi et al., CRYSTAL06 User's Manual, University of Torino (2006).
21. R. Dovesi, R. Oriando, C. Roetti et al., Phys. Stat. Sol. **217**, 63 (2000).
22. http://www.tcm.phy.cam.ac.uk/.
23. J. Perdew, K. Burke, and M. Ernzerhof, Phys. Rev. Lett. **77**, 3865 (1996).
24. A. D. Becke, Phys. Rev. A **38**, 3098 (1988).
25. M. S. Dhaka, U. Paliwal, G. Sharma et al., J. Alloys Comp. **501**, 136 (2010).
26. V. Vyas, R. Kumar, M. C. Mishra et al., Phys. Scripta **84**, 025601 (2011).
27. G. Sharma, M. Sharma, M. C. Mishra et al., Phys. Stat. Sol. (b) **246**, 2263 (2009).
28. M. S. Dhaka, G. Sharma, K. B. Joshi et al., Physica B **405**, 3537 (2010).
29. Z. M.-Xiu, H. K.-Hua, Z. Guang, and H. S. En, Chinese J. Struct. Chem. **27**, 1181 (2008).
30. R. Kumar, M. C. Mishra, B. K. Sharma et al., Comp. Mat. Sci. **61**, 150 (2012).